Angle-resolved electron energy-loss spectroscopy investigation of crystal-field transitions on MnO and NiO surfaces: Exchange scattering versus direct scattering

F. Müller and S. Hüfner

Institut für Experimentalphysik, Naturwissenschaftlich-Technische Fakultät II, Physik und Mechatronik, Universität des Saarlandes, 66123 Saarbrücken, Germany

(Received 21 May 2008; revised manuscript received 2 June 2008; published 28 August 2008)

In electron energy-loss spectroscopy, the excitation of low energy transitions, such as the crystal-field transitions in 3*d* transition-metal oxides, takes place via two scattering mechanism, namely, direct scattering and exchange scattering. The angular cross sections of both scattering mechanisms have been investigated by angular resolved electron energy-loss spectroscopy by comparing the angular intensity distributions of the crystal-field transitions on MnO and NiO. In MnO, the spin-forbidden sextet quartet are excited only by electron exchange scattering with nonuniform cross sections, resulting in nearly isotropic angular intensity distributions for extended energy-loss ranges. In NiO, the excitation of the spin-allowed triplet-triplet transitions is also possible by direct scattering for which the forward scattering is additionally modulated by the reciprocal surface lattice. The angular intensity distributions for extended energy-loss ranges in NiO display a large low-energy electron diffraction-like anisotropy from direct scattering on a broad exchange-scattering background.

DOI: 10.1103/PhysRevB.78.085438 PACS number(s): 79.20.Uv, 71.70.Ch, 72.80.Ga, 73.50.Bk

I. INTRODUCTION

Transition-metal (TM) compounds represent a class of materials of great interest due to their exceptional properties, related to the electronic structure of these strongly correlated systems, as, e.g., the large magnetoresistance in the manganites or the superconductivity of the cuprates.[1] In the special case of the 3*d* TM compounds, the 3*d* TM (mon)oxides, such as NiO, CoO, and MnO, represent systems, where the localized 3*d* electrons can be described in a simple atomiclike picture, namely, by crystal-field (CF) model of Bethe.[2] Within this approach, the solid around the TM ions is approximated by the potential of the adjacent oxygen ligands, which are treated as point charges. Due to the breaking of the symmetry by the crystal field, the one-particle as well as the *n*-particle eigenfunctions of a given $3d^n$ multiplet split into the irreducible representations of the actual point symmetry (in the case of the 3*d* TM monoxides with rock salt structure, O_h symmetry for bulk coordinated TM ions, C_{4v} symmetry for surface coordinated TM ions). These $3d^n$-$3d^n$ CF transitions are especially suited for exploring spin-allowed and spin-forbidden transitions.

CF transitions have been investigated by a large variety of experimental techniques as, e.g., by optical-absorption spectroscopy,[3–5] by electron energy-loss spectroscopy (EELS),[6–16] and recently by resonant or nonresonant inelastic x-ray scattering (RIXS, NIXS).[17–20]

Although in optical-absorption spectroscopy, the *d*-*d* transitions are forbidden by parity selection rules (even symmetry of initial and final states, odd symmetry of the dipole operator) as well as by spin selection rules (as, e.g., for the $\Delta S=-1$ transitions in NiO, CoO, and MnO); the optical spectra however exhibit distinct structures. Parity selection rules can be partially lifted by lattice distortions (Jahn Teller effect, Van-Vleck mechanism) and/or by contributions of multipoles of higher order. Spin selection rules can be relaxed by, e.g., spin-orbit coupling. Nevertheless, the CF intensities, as observed by optical absorption, are small compared to the intensities beyond the optical gap.[3–5]

In contrast to optical-absorption spectra, EELS spectra of these compounds exhibit very strong CF intensities due to the different scattering mechanisms of the probing electrons. Especially from the numerous spin polarized EELS (CSPEELS) investigations by Fromme *et al.*,[6–11,21] it is known, that the excitation of the *d*-*d* transitions takes place by two scattering mechanisms: First, direct (dipole) scattering acts as a long-range interaction, and only spin-allowed transitions with $\Delta S=0$ can be excited. Second, electron exchange scattering acts as a short-range interaction at the local 3*d* TM site, and due to the exchange of the primary electron and a target electron, spin selection rules are no longer restricted to the target electrons. Spin-forbidden transitions with $\Delta S\neq 0$ can be excited if both, the spin of the primary/scattered electron and the spin of the target, are taken into account. For example, the $3d^5$ configuration of MnO provides only spin-forbidden sextet-quartet transitions because of the high spin ground state, and therefore, these transitions are displayed mainly in the spin-flip part of the CSPEELS spectrum (cf. Fig. 4 of Ref. 6).

With respect to the angular distributions of the scattering cross sections, the CSPEELS investigations by Fromme *et al.*[21] gave evidence that exchange scattering is *angularly wide spread*, whereas direct scattering is *sharply peaked around specular scattering geometry*.[7,21] Due to the complexity of the method, the investigations of scattering cross sections by CSPEELS were restricted to a small angular range around specular scattering geometry.

In angular resolved EELS (AREELS) experiments on NiO(001),[12,13] the angular intensity distributions of the CF transitions were investigated within the whole 2π hemisphere above the surface of the sample. The results were in full accordance to the CSPEELS experiments, but due to the wider angular range, the AREELS experiments provided additional information. With respect to direct scattering, the

angular intensity distributions of the spin-allowed triplet-triplet transitions (excited by both, exchange scattering as well as direct scattering) gave evidence that the specular direction just represents a special case of a more general scattering geometry, namely, low-energy electron diffraction (LEED)-like scattering. For example, on the (100) symmetry axis, the intensity distribution of the 1.6 eV loss in NiO ($^3A_{2g} \rightarrow {}^3T_{1g}$) exhibits maxima along the (00) reflection (specular direction) and along the (11) reflection (cf. Fig. 4 in Ref. 12). In contrast, the intensity distributions of the triplet-singlet transitions, which are excited by electron exchange scattering exclusively, did not show such LEED-like intensity contributions and each triplet-singlet transition displayed an individual exchange-scattering cross section.

In this study, the cross sections of direct and exchange scatterings are investigated by comparing the polar intensity distributions of the $3d$-$3d$ CF transitions in NiO and MnO along the (100) and (110) symmetry directions in the full angular range. In a first attempt, the cross sections have been investigated for extended energy-loss ranges (i.e., several transitions contribute to the overall cross sections) in order to find out the main differences between both scattering mechanism.

Despite the general interest in the angular features of both scattering mechanisms as, e.g., for a comparison of spectral intensities with calculated oscillator strengths, a detailed knowledge of especially the exchange-scattering mechanism may provide useful information with regard to future applications in technology as, e.g., in spin electronic devices. In such a device, the logical bit may be represented by the spin of a single electron, and a loss of information by a spin flip due to the exchange of the "storage" electron with an electron from, e.g., the driving current, must not take place.

II. EXPERIMENT

The experimental setup was described in detail in Refs. 12, 13, and 22. The experiments were performed with a VG ESCA Mk II spectrometer, which is designed for angular resolved photoelectron spectroscopies such as x-ray photoelectron diffraction (XPD) and angle-resolved ultraviolet photoemission spectroscopy (ARUPS). The sample can be rotated by a two-axes manipulator (polar angle ϑ, azimuthal angle φ), so that the electron analyzer can detect the whole 2π hemisphere above the surface of the sample. For the present AREELS investigations, the sample was tilted in the scattering plane (spanned by the surface normal of the sample and the entrance axis of the analyzer) along the (100) and (110) directions of the epitaxially grown NiO/Ag(001) and MnO/Ag(001) samples. The electron gun [thermal electron source, full width at half maximum (FWHM) $\sim$230 meV] is mounted on a goniometer and can be tilted within the scattering plane to vary the scattering angle α (in the present case, α was fixed at 123°). The setup is shown in Fig. 1.

The NiO/Ag(001) and MnO/Ag(001) samples were prepared following the recipes described Refs. 12, 13, and 22. Briefly, Ni or Mn was evaporated from rods by a modified e^--beam evaporator by Oxford Applied Research within an

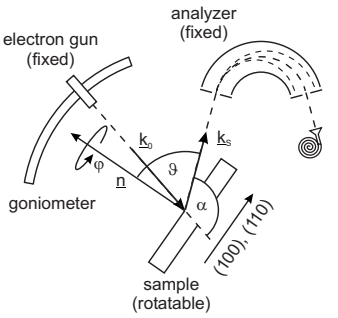

FIG. 1. Experimental setup as described in the text.

appropriate oxygen atmosphere. The growth rate was of the order of 1 monolayer per minute. For the samples used in this study, the thickness of the TMO films exceeded the probing depth in XPS, i.e., no $3d$ core-level intensities from the Ag substrate were detected. With respect to the enhanced surface sensitivity in EELS (for primary energies in the range of 30 eV, the kinetic energies of the investigated energy-loss ranges are close to the minimum of the so-called "universal curve" of the electron mean-free path), the samples therefore represented semi-infinite single crystals.

III. RESULTS AND DISCUSSION

Figure 2 shows the EELS spectra of NiO and MnO for arbitrary scattering geometries away from scattering through a surface reciprocal-lattice vector, i.e., in order to reduce the tails of the elastic intensity, the transfer of momentum

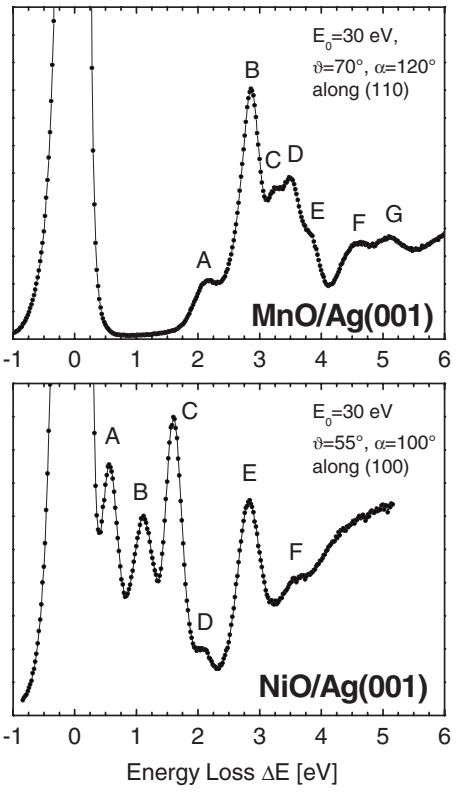

FIG. 2. EELS spectra of MnO/Ag(001) and NiO/Ag(001).

TABLE I. *d-d* excitation energies (in eV) for MnO.

Transition $^6A_{1g}(G)\rightarrow$	Optical	Optical	Optical	EELS	EELS	(CSP) EELS	LFT[a]	EELS
$^4T_{1g}(G)$	2.03	1.97	2.03	2.0	2.2	2.13	2.01	2.16 (A)
$^4T_{2g}(G)$	2.58	2.51	2.55	-	-	2.4	2.56	2.86 (B)
$^4E_g/^4A_{1g}(G)$	2.95	2.94	2.97	2.9	2.8	2.82	2.95	3.25 (C)
$^4T_{2g}$(D)	-	3.21	3.29	3.4	3.4	3.31	3.50	3.50 (D)
^4E_g(D)	-	3.46	3.48	-	-	3.82	3.69	3.83 (E)
$^4T_{1g}(P)$	-	-	-	-	4.6	4.57	4.20	4.63 (F)
$^4A_{2g}(F)$	-	-	-	-	-	5.08	-	5.13 (G)
$^4T_{1g}(F)$	-	-	-	-	-	5.38	-	-
Reference	3	4	24	16	15	6	25	23

[a]LFT: ligand field theory.

$\underline{q}^2=(\underline{k}_s-\underline{k}_0)^2\sim 2\cdot E_0\cdot(1-\Delta E/(2E_0)-\sqrt{1-\Delta E/E_0}\cos\alpha)$ does not match with a reciprocal (surface) lattice vector within the whole energy-loss range ΔE (for the influence of the scattering geometry, cf. Figure 3 in Ref. 12). Both spectra exhibit all prominent loss structures which are known for NiO and MnO. Tables I and II give a survey of the peak assignment as proposed by various authors (in both cases, there are slight differences with respect to the observed energies as well as with respect to the interpretation of the peaks).

For NiO, the CF transitions are classified as bulk (O_h coordination of the Ni ion) and surface related transitions (C_{4v} coordination) because here, surface states are well known. They have been identified by their response to the presence of adsorbates[14] as well as by their varying spectral weight for different thicknesses of epitaxially grown NiO films.[13] For MnO, the CF transitions are assigned only to the bulk related states because (to our knowledge) surface states have not been reported so far (from quantum chemical *ab initio* calculations it is known that in MnO, surface and bulk states differ only by few meV,[23] and therefore, a separation of surface and bulk states would be possible only by enhanced resolutions).

From Fig. 2 it is also evident, that the investigation of the angular cross sections of the individual CF transitions of MnO as, e.g., performed for NiO,[12,13] is much more difficult or even impossible by resolutions in the range of 230 meV (as presented here), because the loss structures exhibit a strong overlap. In order to investigate exchange scattering and direct scattering by comparing the angular intensity distributions of NiO and MnO, we therefore have to rely (at least for a first approach) on combined energy-loss ranges, i.e., the angular intensity is recorded for extended energy-loss ranges, containing several CF transitions. This procedure is based on the following ideas.

(i) According to the data in Tables I and II, there is no need to know exactly what kind of transition is assigned to a particular energy loss. For NiO, one knows that both, spin-allowed triplet-triplet transitions as well as spin-forbidden triplet-singlet transitions, contribute to the overall intensity of each energy-loss range. Therefore, the angular intensity

TABLE II. *d-d* excitation energies (in eV) for NiO.

Transition (Bulk) $^3A_{2g}\rightarrow$	Transition (Surface) $^3B_1\rightarrow$	EELS	Calculated (VCI[a], MC-CEPA[b])	Calculated (R matrix)	EELS	Optical	CSPEELS
	^1E	0.6 (A)	0.54–0.65	-	-	-	0.6
	$^3B_2$	1.1 (B)	0.86–1.00	-	-	-	1.1
$^3T_{2g}$		1.1 (B)	0.86–1.00	1.05	1.05–1.07	1.13	1.1
	$^3A_2$	1.1 (B)	1.11–1.30	-	-	-	1.3
^1E_g		1.6 (C)	-	1.60	1.66–1.70	1.75	1.6
$^3T_{1g}$		1.6 (C)	1.50–1.81	1.70	1.79–1.84	1.95	1.6
	^1E	2.1 (D)	-	-	-	2.15	2.1
$^1T_{2g}$		2.7 (E)	-	2.70	-	2.75	2.7
$^1A_{1g}$		2.7 (E)	-	2.80	-	3.25	-
$^3T_{1g}$		-	-	3.13	2.90–3.00	2.95	-
$^1T_{1g}$		3.5 (F)	-	3.28	-	3.52	-
Reference		13	14	26	27	5	8

[a]VCI: valence configuration interaction.

[b]MC-CEPA: multiconfiguration coupled electron pair approximation.

distributions display a superposition of direct and exchange-scattering cross sections. For MnO, one knows that only spin-forbidden sextet-quartet transitions contribute to the overall intensity of each energy-loss range. Therefore, the angular intensity distributions just display a superposition of exchange-scattering cross sections.

(ii) If, according to the results of spin polarized CSPEELS and angular resolved AREELS investigations, exchange scattering exhibits nonuniform cross sections that are distributed over a wide angular range, then, the overall exchange-scattering cross section of several transitions should average to a smooth isotropic overall distribution (with the degree of anisotropy depending on the number of transitions and the relative strength of each cross section).

(iii) If, according to the results from the AREELS investigations, direct scattering is denoted to provide a uniform LEED-like cross section, independent on the particular transition, then all direct-scattering contributions of the spin-allowed transitions within a combined energy-loss range are expected to add to a common LEED-like intensity distribution.

(iv) For MnO, as a pure exchange-scattering system (only sextet-quartet transitions), the angular intensity distributions are therefore expected to exhibit smooth angular shapes. In contrast, for NiO, representing a direct (triplet-triplet transitions) as well as a exchange-scattering system (triplet-singlet transitions and triplet-triplet transitions), a LEED-like intensity distribution from direct scattering upon a smooth exchange-scattering "background" is expected.

Figures 3 and 4 show the scattering distributions for MnO and NiO. In the EELS spectra of the left column of each figure, it is shown how the loss intensities contribute to the angular intensity distributions along the (100) symmetry axis (middle column) and the (110) axis (right column), respectively. For the LEED scattering of the elastic electrons (upper row), the overall intensity of the elastic peak at $\Delta E=0$ was recorded (the shaded area in the EELS spectrum on the left corresponds to the FWHM of about 230 meV. The red dashed lines represent the LEED spots for $\alpha=123°$ and $|\underline{k}_0|/[\text{Å}]=0.512\sqrt{E_0[\text{eV}]}$, $E_0=30$ eV). For the scattering of the CF transitions (middle row and lower row), the intensity was determined by a linear background subtraction.

For MnO, the inelastic scattering of the CF transitions just displays the cross sections of electron exchange because only spin-forbidden sextet-quartet transitions contribute to the overall intensities of the selected energy-loss ranges.

The angular intensity distributions of the elastically scattered electrons in Figs. 3(b) and 3(c) exhibit sharp LEED reflections with no background intensities, indicating that MnO/Ag(001) forms a well-ordered epitaxial layer, but compared to NiO (see below) and the clean Ag(001) substrate (not shown), the peak widths are slightly enhanced due to the large lattice mismatch of about 9%.

For the energy-loss range from ~1.6 eV to about ~4.2 eV [Fig. 3(d)], six exchange-scattering cross sections ($^6A_{1g}\rightarrow{}^4T_{1g}$, $2\cdot{}^4T_{2g}$, $2\cdot{}^4E_g$, $^4A_{1g}$, cf. Table I) contribute to the angular intensity distributions in Figs. 3(e) and 3(f). The polar intensity plots exhibit nearly no angular anisotropies, and in both cases, the overall shape of the scattering distributions is quite similar to the blue dotted lines. Since these lines represent the angular intensity distribution of the elastic electrons as scattered at the surface of a polycrystalline Ag film grown on a glass substrate, they display the angular transmission of the setup without any intrinsic angular effects caused by the sample. Therefore, the observation of very weak anisotropies in Figs. 3(e) and 3(f) gives evidence that (ii) is valid due to the large number of contributing CF transitions. Although these polar intensity plots do not provide any detailed information of the individual exchange cross sections, the resemblance of the overall intensity distributions and the angular transmission of the setup show that the contributing CF transitions do not exhibit uniform cross sections. Otherwise, common features would cause larger anisotropies.

The situation is slightly different for the energy-loss range from ~4.2 to ~5.6 eV in Fig. 3(g). According to Table I, only three CF transitions ($^6A_{1g}\rightarrow{}^4A_{2g}, 2\cdot{}^4T_{1g}$) contribute to the exchange cross sections in Figs. 3(h) and 3(i) and in contrast to the preceding case, the angular anisotropies are now clearly enhanced. Especially along the (110) axis, the scattering distribution displays individual structures that are (as expected for exchange scattering) extended over a broad angular range.

At this stage, the most important information, which is provided by the inelastic polar intensity plots, is that the combined exchange cross sections do not exhibit distinct maxima along the LEED directions.

For NiO, the combined scattering intensities of the spin-allowed triplet-triplet transitions and the spin-forbidden triplet-singlet transitions display both the cross sections of direct scattering as well as the cross section of exchange scattering.

The scattering of the elastic electrons in Figs. 4(b) and 4(c) exhibits sharp LEED reflections without any background intensities, i.e., NiO/Ag(001) also forms a well-ordered epitaxial layer [compared to MnO, the peak widths are clearly reduced, indicating that the average domain size for NiO/Ag(001) is larger than for MnO/Ag(001), cf. lattice mismatch NiO/Ag(001): 2% vs MnO/Ag(001): 9%].

According to Table II, two direct as well as three exchange-scattering cross sections ($^3A_{2g}\rightarrow{}^3T_{2g}, {}^3T_{1g}, {}^1E_g$) contribute to the energy-loss range from ~0.8 to ~2.0 eV in Fig. 4(d). The corresponding polar intensity distributions along the (100) and (110) axes in Figs. 4(e) and 4(f) are now formed by two contributions: First, similar to MnO, there is a broad angular "background." Second, in contrast to MnO, the intensities are additionally sharply peaked, similar to the scattering of the elastic electrons. For both axes, there is a strong intensity along the (00) LEED spot, representing the forward scattering, as reported in Ref. 7. In addition, the intensity distribution along the (100) axis [Fig. 4(e)] also exhibits a sharp peak along the (11) spot, while the intensity distribution along the (110) axis displays a peak along the (10) spot [and, to some restriction, it also displays a diffuse peak along the $(\bar{1}0)$ spot]. If, according to the results for MnO, the broad background intensities are assigned to the contributions from the exchange scattering of the $^3A_{2g}\rightarrow{}^3T_{2g}$, $^3T_{1g}$, ^1E_g transitions, then the LEED-like scattering has to be assigned to the superposition of the direct-

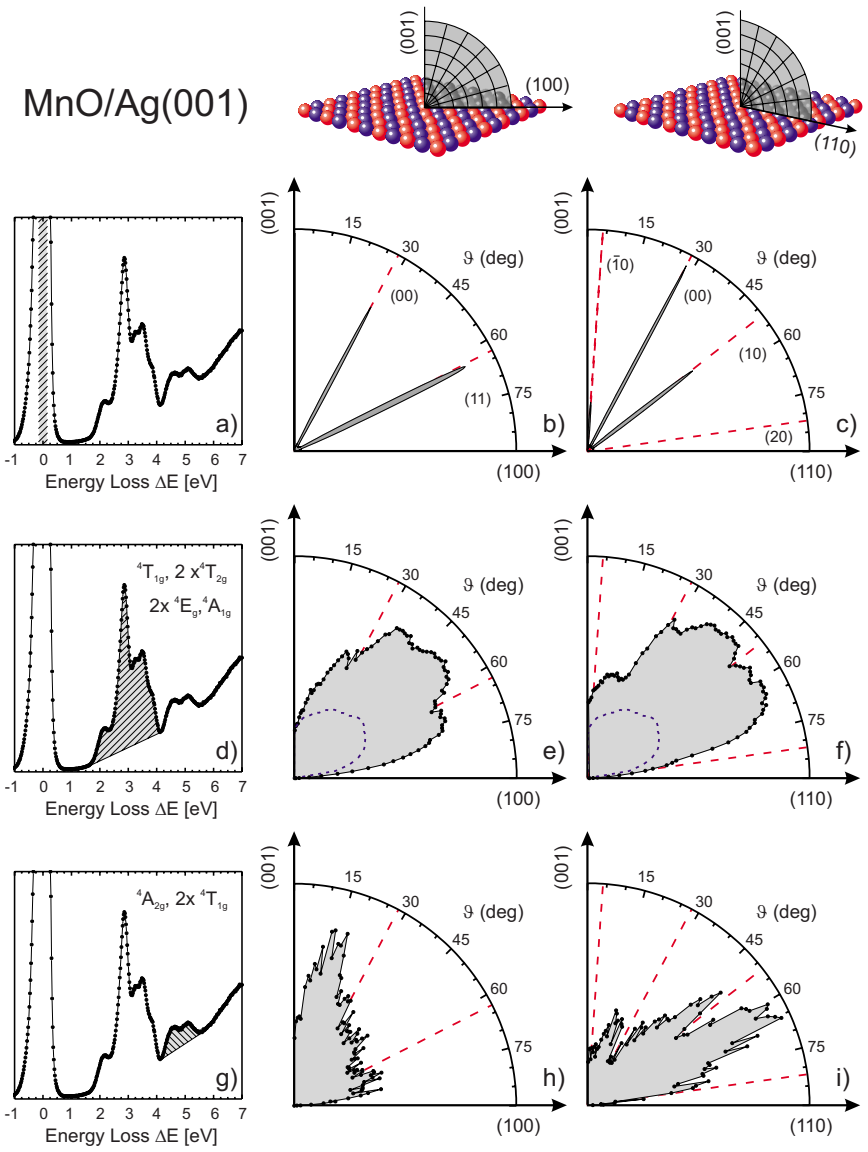

FIG. 3. (Color online) Elastic and inelastic-scattering distributions for MnO/Ag(001), E_0=30 eV, and α=123°. (a) Elastic intensity at ΔE=0 with FWHM ~ 230 meV. (b) Polar LEED distribution for the elastic electrons from (a) along (100). Red dashed lines represent the LEED directions. Spots are labeled by the reciprocal surface lattice. The surface normal is along the (001) axis. (c) Same as (b) along the (110) axis. (d) First group of CF transitions of MnO, ranging from 1.6 to 4.2 eV. (e) Polar intensity distributions of energy-loss range from (d) along (100). The blue dotted lines represent the angular transmission of the setup (see text). (f) Same as (e) along the (110) axis. (g) Second group of CF transitions of MnO, ranging from 4.2 to 5.6 eV. (h) Same as (e) for energy-loss range from (g). (i) Same as (f) for energy-loss range from (g).

scattering contributions of the $^3A_{2g} \rightarrow {}^3T_{2g}$, $^3T_{1g}$ transitions.

This interpretation is then also in accordance to the results for the remaining part of the NiO spectrum, namely, the energy-loss range from ~2.5 to ~4.2 eV [Fig. 4(g)]. Now, the excitation of the $^3A_{2g} \rightarrow {}^3T_{1g}$, $^1T_{2g}$, $^1T_{1g}$, $^1A_{1g}$ transitions mainly takes place by electron exchange (one direct-scattering channel vs four exchange-scattering channels), and therefore, the LEED-like contributions from direct scattering are expected to be smaller as in the preceding case. Indeed, for both axes, the scattering distributions in Figs. 4(h) and 4(i) mainly exhibit broad angular features, as characteristic for the exchange-scattering cross sections, even with distinct minima along the LEED directions. Nevertheless, there is still a small, sharp contribution of a LEED-like (00) spot along the (100) axis, resulting from the direct scattering of the $^3A_{2g} \rightarrow {}^3T_{1g}$ transition, as depicted in the inset of Fig. 4(h). This (00)-like spot has no counterpart along the (110) axis in Fig. 4(i).

The comparison of the angular intensity distributions of the CF transitions on epitaxial NiO and MnO films over a wide angular range provided useful information about some general characteristics of the scattering mechanisms involved in the excitation of these *d-d* transitions, namely, direct and exchange scatterings.

Although these experiments do not provide detailed information about the individual exchange-scattering cross sec-

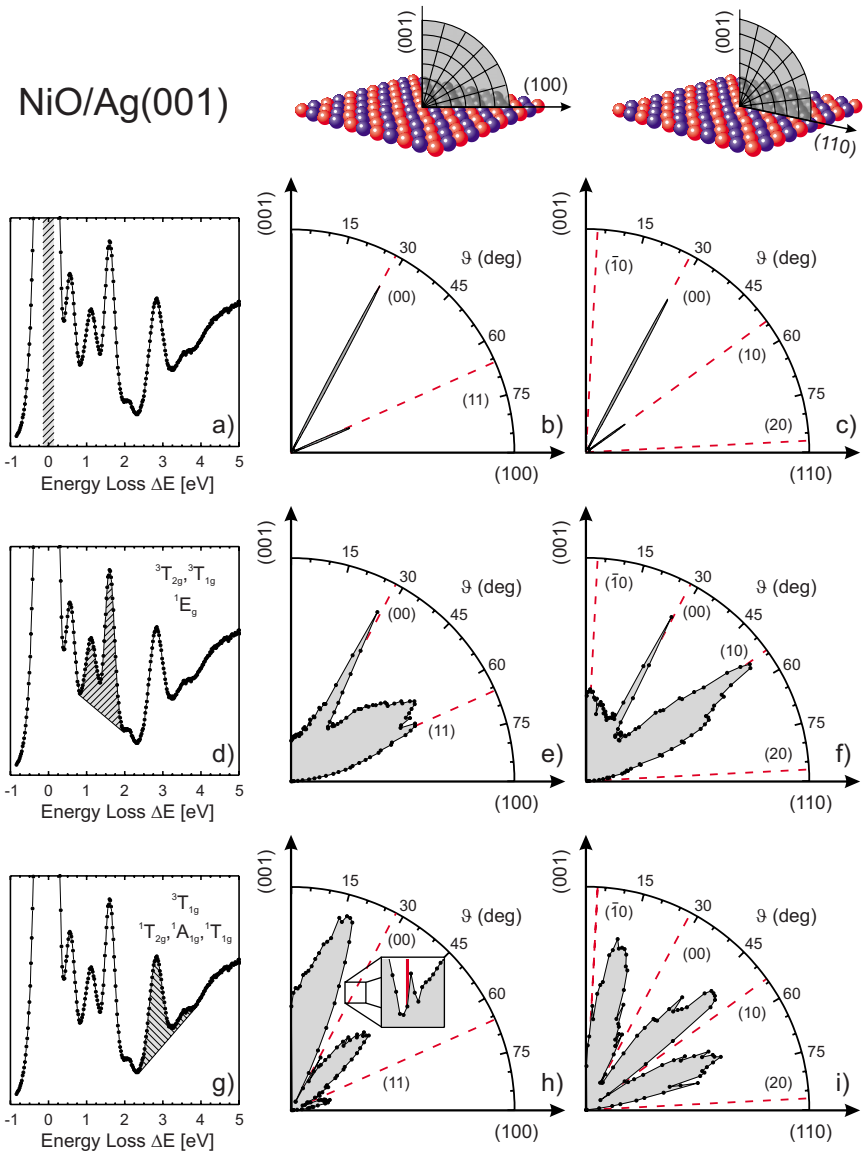

FIG. 4. (Color online) Elastic and inelastic-scattering distributions for NiO/Ag(001), E_0=30 eV, and α=123°. (a) Elastic intensity at ΔE=0 with FWHM ~ 230 meV. (b) Polar LEED distribution for the elastic electrons from (a) along (100). Red dashed lines represent the LEED directions. Spots are labeled by the reciprocal surface lattice. The surface normal is along the (001) axis. (c) Same as (b) along the (110) axis. (d) First group of CF transitions of NiO, ranging from 0.8 to 2.0 eV. (e) Polar intensity distributions of energy-loss range from (d) along (100). (f) Same as (e) along the (110) axis; (g) Second group of CF transitions of NiO, ranging from 2.5 to 4.2 eV. (h) Same as (e) for energy-loss range from (g). (i) Same as (f) for energy-loss range from (g).

tions (because only combined cross sections were investigated), the results give some evidence that direct scattering displays uniform LEED-like cross sections, i.e., the dipole-like forward scattering is additionally modulated by the reciprocal lattice.

In a next step, it would be interesting to investigate the individual exchange-scattering cross sections on MnO in detail by full hemispherical intensity maps, similar to the case of NiO in Refs. 12 and 13, but to our present knowledge, such an attempt is not expected to be successful. In contrast to NiO, the separation of surface and bulk states on MnO is often in the range of only a few meV (Ref. 23) and therefore, even experiments with enhanced energy resolution would hardly provide information beyond those of the present study. Of course, it would be possible to reduce the number of the transitions that contribute to a given energy-loss range, but at least, the corresponding angular intensity distribution would display rather a superposition of two or three exchange-scattering cross sections than the cross section of an individual transition. Details about surface states on MnO will be presented in a later study.[23]

IV. SUMMARY

The cross sections of direct scattering and electron exchange scattering have been investigated with angular resolved EELS spectroscopy by comparing the angular intensity distributions of the CF transitions on NiO and MnO over

the full angular range, at least for the main symmetry axes along (100) and (110), respectively.

For MnO, the excitation of the spin-forbidden sextet-quartet transitions takes place only by electron exchange scattering, and therefore, the angular intensity distributions, taken for extended energy-loss ranges, directly display the combined cross sections for electron exchange. Depending on the number of the transitions, which contribute to the overall intensity, the combined exchange cross sections display broad angular features or average to a smooth, nearly isotropic intensity distribution, i.e., the individual exchange cross sections do not provide common angular characteristics.

For NiO, the excitation of the spin-allowed triplet-triplet transitions takes place by direct as well as by electron exchange scatterings, while the spin-forbidden triplet-singlet transitions are excited only by electron exchange. Similar to MnO, the angular intensity distributions display a broad angular background, as related to the exchange scattering, but in addition, the intensity distributions also display a LEED-like scattering contribution, which can be assigned to the contributions from direct scattering.

In order to prove the validity of these results, future investigations on other TM oxides, as, e.g., CoO, are required. For CoO, the situation is similar to NiO: The quartet-quartet transitions are excited by direct as well as electron exchange scatterings, while the quartet-doublet transitions are excited only by electron exchange. Therefore, the scattering distributions of the CF transitions on CoO are expected to provide the same angular features as in the case of NiO, i.e., a LEED-like intensity distribution from direct scattering upon a broad angular background from exchange scattering should be observed.

For a detailed investigation of the angular characteristics of exchange-scattering cross sections as, e.g., with respect to the dependence on the final-state symmetry, MnO would represent an ideal prototype system because exchange scattering is displayed directly by the experimental intensity distributions, i.e., there is no impact by contributions from direct scattering as in the case of NiO or CoO. Unfortunately, MnO represents also a system for which bulk states and surface states differ only by a few meV, and therefore, AREELS investigations of the individual CF transitions on MnO, as reported for NiO in Refs. 12 and 13, are hardly possible.

ACKNOWLEDGMENTS

This work has been supported by the Deutsche Forschungsgemeinschaft through SFB 277 "Grenzflächenbestimmte Materialien," TP B5. The authors thank V. Staemmler, Ruhr-Universität, Bochum, for providing information about the surface states on MnO prior to publication.

[1] M. Imada, A. Fujimori, and Y. Tokura, Rev. Mod. Phys. **70**, 1039 (1998).
[2] H. Bethe, Ann. Phys. **5**, 133 (1929).
[3] G. W. Pratt and R. Coelho, Phys. Rev. **116**, 281 (1959).
[4] D. R. Huffman, R. L. Wild, and M. Shinmei, J. Chem. Phys. **50**, 4092 (1969).
[5] R. Newman and R. M. Chrenko, Phys. Rev. **114**, 1507 (1959).
[6] B. Fromme, U. Brunokowski, and E. Kisker, Phys. Rev. B **58**, 9783 (1998).
[7] B. Fromme, M. Möller, C. Bethke, U. Brunokowski, and E. Kisker, Phys. Rev. B **57**, 12069 (1998).
[8] B. Fromme, M. Möller, Th. Anschütz, C. Bethke, and E. Kisker, Phys. Rev. Lett. **77**, 1548 (1996).
[9] B. Fromme, Ch. Koch, R. Deussen, and E. Kisker, Phys. Rev. Lett. **75**, 693 (1995).
[10] B. Fromme, M. Schmitt, E. Kisker, A. Gorschlüter, and H. Merz, Phys. Rev. B **50**, 1874 (1994).
[11] B. Fromme, *d-d Excitations in Transition Metal Oxides*, Springer Tracts in Modern Physics Vol. 170 (Springer, Berlin, 2001).
[12] F. Müller, P. Steiner, Th. Straub, D. Reinicke, S. Palm, R. de Masi, and S. Hüfner, Surf. Sci. **442**, 485 (1999).
[13] F. Müller, R. de Masi, P. Steiner, D. Reinicke, M. Stadtfeld, and S. Hüfner, Surf. Sci. **459**, 161 (2000).
[14] A. Freitag, V. Staemmler, D. Cappus, C. A. Ventrice, Jr., K. Al Shamery, H. Kuhlenbeck, and H.-J. Freund, Chem. Phys. Lett. **210**, 10 (1993).
[15] S.-P. Jeng and V. E. Henrich, Solid State Commun. **82**, 879 (1992).
[16] J. P. Kemp, S. T. P. Davis, and P. A. Cox, J. Phys.: Condens. Matter **1**, 5313 (1989).
[17] G. Ghiringhelli, M. Matsubara, C. Dallera, F. Fracassi, A. Tagliaferri, N. B. Brookes, A. Kotani, and L. Braicovich, Phys. Rev. B **73**, 035111 (2006).
[18] G. Ghiringhelli, M. Matsubara, C. Dallera, F. Fracassi, R. Gusmeroli, A. Piazzalunga, A. Tagliaferri, N. B. Brookes, A. Kotani, and L. Braicovich, J. Phys.: Condens. Matter **17**, 5397 (2005).
[19] S. G. Chiuzbaian, G. Ghiringhelli, C. Dallera, M. Grioni, P. Amann, X. Wang, L. Braicovich, and L. Patthey, Phys. Rev. Lett. **95**, 197402 (2005).
[20] B. C. Larson, W. Ku, J. Z. Tischler, C. C. Lee, O. D. Restrepo, A. G. Eguiluz, P. Zschack, and K. D. Finkelstein, Phys. Rev. Lett. **99**, 026401 (2007).
[21] B. Fromme, V. Bocatius, and E. Kisker, Phys. Rev. B **64**, 125114 (2001).
[22] F. Müller, R. de Masi, D. Reinicke, P. Steiner, S. Hüfner, and K. Stöwe, Surf. Sci. **520**, 158 (2002).
[23] F. Müller, S. Hüfner, N. Rössler, V. Staemmler (unpublished).
[24] R. N. Iskenderov, I. A. Drabkin, L. T. Emel'yanova, and Ya. M. Ksendzov, Sov. Phys. Solid State **10**, 2031 (1969).
[25] J. van Elp, R. H. Potze, H. Eskes, R. Berger, and G. A. Sawatzky, Phys. Rev. B **44**, 1530 (1991).
[26] J. J. M. Michiels, J. E. Inglesfield, C. J. Noble, V. M. Burke, and P. G. Burke, Phys. Rev. Lett. **78**, 2851 (1997).
[27] P. A. Cox and A. A. Williams, Surf. Sci. **152-153**, 791 (1985).